Earth and Planetary Science Letters 515 (2019) 100–111

Contents lists available at ScienceDirect

Earth and Planetary Science Letters

www.elsevier.com/locate/epsl

Post-depositional overprinting of chromium in foraminifera

Serginio R.C. Remmelzwaal [a,*], Aleksey Yu. Sadekov [b,c], Ian J. Parkinson [a], Daniela N. Schmidt [a], Danna Titelboim [d], Sigal Abramovich [d], Anne Roepert [e], Michiel Kienhuis [e], Lubos Polerecky [e], Heather Goring-Harford [f], Katsunori Kimoto [g], Katherine A. Allen [h], Kate Holland [i], Joseph A. Stewart [a], Jack J. Middelburg [e]

[a] School of Earth Sciences, University of Bristol, Wills Memorial Building, Queens Road, Bristol BS8 1RJ, United Kingdom
[b] Department of Earth Sciences, University of Cambridge, Downing Street, Cambridge CB2 3EQ, United Kingdom
[c] School of Earth Sciences, University of Western Australia, 35 Stirling Highway, Crawley WA 6009, Australia
[d] Department of Geological and Environmental Sciences, Ben-Gurion University of the Negev, Mailbox 653, Beer-Sheva 84105, Israel
[e] Department of Earth Sciences, Faculty of Geosciences, Utrecht University, P.O Box 80.021, 3508 TA Utrecht, the Netherlands
[f] Ocean and Earth Science, National Oceanography Centre Southampton, University of Southampton, European Way, Southampton SO14 3ZH, United Kingdom
[g] Research Center for Global Change (RCGC), Japan Agency for Marine-Earth Science and Technology (JAMSTEC), Yokosuka, Japan
[h] School of Earth and Climate Sciences, University of Maine, 5790 Bryand Global Sciences Center, Orono, ME 04469-5790, United States of America
[i] Research School of Earth Sciences, The Australian National University, 2601 Canberra, ACT, Australia

ARTICLE INFO

Article history:
Received 28 October 2018
Received in revised form 27 February 2019
Accepted 1 March 2019
Available online 28 March 2019
Editor: D. Vance

Keywords:
chromium
foraminifera
diagenesis
distribution coefficient
laser ablation
nanoSIMS

ABSTRACT

Present-day ocean deoxygenation has major implications for marine ecosystems and biogeochemical cycling in the oceans. Chromium isotopes are used as a proxy to infer changes in past oceanic redox state. Chromium isotopes in carbonates, including the prime proxy carrier foraminifera, were initially thought to record the seawater composition during crystallisation. However, the uptake of Cr into foraminiferal tests and carbonates is still poorly understood and recent studies question this assumption. We assess whether Cr in foraminiferal calcite is taken up during biomineralisation, has a post-depositional origin or is a combination of the two. Laser Ablation-MC-ICP-MS analyses and NanoSIMS imaging of individual tests were used to characterise the distribution of Cr in both planktic and benthic foraminifera. Foraminifera in sediment core-top samples have up to two orders of magnitude more Cr than sediment trap, plankton net, and culture samples. In cultured specimens, Cr is incorporated in foraminiferal tests at low concentrations (0.04–0.13 ppm) with a distribution coefficient of ~250 ± 43 (2SE) which is an upper estimate due to substantial loss of dissolved Cr during the experiment. Part of the Cr signal in sedimentary foraminifera may be primary, but this primary signal is likely often overprinted by the uptake of Cr from bottom and pore waters. In sediment samples, there is no significant isotopic offset between individual species and bulk foraminiferal calcite from the same size fraction. The >500 µm fraction has a heavier isotopic composition than the smaller 250–500 µm fraction with an offset of −0.3 to −0.5‰ due to an increase in surface area to volume. We propose that Cr in foraminifera is predominantly post-depositional and records bottom/pore water signals. This is contrary to current interpretations of the foraminiferal Cr isotope proxy as a surface seawater redox proxy.

1. Introduction

Anthropogenic global warming has caused dissolved oxygen levels in the oceans to drop globally by 2% over the past decades (Schmidtko et al., 2017). This loss of oxygen is projected to continue at up to −0.64 µM per year (Stramma et al., 2012). As ocean deoxygenation threatens marine ecosystems (Keeling et al., 2010), a more robust understanding of the effects of deoxygenation on biogeochemical cycling, the carbon pump and marine life is important. One way of untangling the effects of deoxygenation is by looking at the response during past climate perturbations.

Chromium occurs in two valence states in the marine environment, Cr(III) and Cr(VI), and is therefore sensitive to redox changes (e.g. Elderfield, 1970; Cranston and Murray, 1978; Bonnand et al., 2013; Reinhard et al., 2014; Wang et al., 2016). In modern well-oxygenated seawater, chromium is predominantly present as Cr(VI)-oxyanions, whereas Cr(III) is insoluble and will adhere to particles, thus forming a sink to the seafloor and deplet-

* Corresponding author.
E-mail address: serginio.remmelzwaal@bristol.ac.uk (S.R.C. Remmelzwaal).

https://doi.org/10.1016/j.epsl.2019.03.001
0012-821X/

ing low-oxygen seawater in Cr (Cranston and Murray, 1978). Recently, phytoplankton have been found to be able to reduce Cr(VI) and could therefore act as an additional sink for Cr in surface waters (Semeniuk et al., 2016). Chromium speciation is redox coupled to Mn and Fe (e.g. Schroeder and Lee, 1975; Cranston and Murray, 1978), and is therefore thought to track oxygenation dynamics in the present and past.

Additional to Cr concentrations, Cr isotopes have been suggested as a way to reconstruct past oxygenation. There are four stable Cr isotopes of which ^{52}Cr and ^{53}Cr are the most abundant, and so stable Cr isotope variations are assessed using the ^{53}Cr/^{52}Cr ratio expressed as $\delta^{53}\mathrm{Cr} = [(^{53}\mathrm{Cr}/^{52}\mathrm{Cr}_{\mathrm{sample}})/(^{53}\mathrm{Cr}/^{52}\mathrm{Cr}_{\mathrm{NBS\ 979}}) - 1] \times 1000$ (e.g. Bonnand et al., 2011). Reduction of Cr(VI) to Cr(III) can produce isotopic fractionation of up to 7‰, enriching the remaining Cr(VI) pool in ^{53}Cr (Ellis et al., 2002), although the isotopic fractionation associated with Cr(VI) reduction is likely smaller in open ocean settings due to less reducing conditions (Scheiderich et al., 2015; Paulukat et al., 2016; Goring-Harford et al., 2018). For O_2 concentrations above 44 µmol kg^{-1} there is no correlation between seawater δ^{53}Cr values and dissolved O_2 content and hence Cr(VI) likely only reduces at oxygen concentrations below this (Goring-Harford et al., 2018). Carbonate chromium isotope ratios are thought to reflect seawater values (Tang et al., 2007; Frei et al., 2011; Bonnand et al., 2013) through the substitution of the carbonate ion by CrO_4^{2-}. Therefore, fossilised remains of marine calcifiers such as foraminifera can act as archives of past climate proxies. To use the foraminiferal chromium records in the past, it is imperative to piece together the origin of chromium in the test and what controls its uptake.

In order to apply a new isotope system to an archive, a number of parameters need to be well established, such as biotic influences on uptake, location of the isotope within the host material, and post-depositional alteration.

Previous studies into the fractionation of Cr isotopes in biogenic carbonates have yielded widely variable results. Scleractinian corals made of aragonite show a large disequilibrium with seawater, resulting in a fractionation from −0.5 to +0.33‰ relative to seawater (Pereira et al., 2016). Bulk carbonate samples of mainly macroalgal origin from the Caribbean, and therefore also likely aragonitic, have Cr isotope values offset from seawater by −0.46‰ (Holmden et al., 2016). A systematic enrichment of lighter Cr isotopes in carbonates relative to seawater was confirmed by a study of biogenic carbonates from several oceanic provinces (Farkaš et al., 2018). A recent study assessing the fractionation associated with Cr uptake by calcitic foraminifera (Wang et al., 2017) concluded that it is unclear whether the chromium isotopic composition of foraminifera reflects surface seawater δ^{53}Cr values, as different species from the same sample site and the same depth habitats showed significant variations in δ^{53}Cr in this study. As the study presented by Wang et al. (2017) analysed multiple species of foraminifera larger than 125 µm, mixing a wide range of sizes, it does not consider any effects that growth rates or species-specific differences in biomineralisation may have on δ^{53}Cr. Post-depositional exchange with bottom and pore waters could alter the δ^{53}Cr isotope composition; size driven changes in foraminiferal surface area to volume ratios (A/V) would facilitate different impacts on the residual values with smaller specimens more prone to this effect. This behaviour has also been observed for Mg (Schmidt et al., 2008).

To fully assess the potential of Cr isotopes in foraminifera as a palaeoproxy, Cr uptake by foraminifera from their ambient environment needs to be determined. Previous estimates of distribution coefficients of Cr ($D_{\mathrm{Cr}} = [\mathrm{Cr}]_{\mathrm{foraminifer}}/[\mathrm{Cr}]_{\mathrm{seawater}}$) in foraminiferal calcite range from approximately 303 to 4000, and are based on core-top planktic foraminifera and seawater Cr concentrations averaged over the Pacific and Atlantic Ocean basins (Wang et al., 2017). Distribution coefficients in other biogenic carbonates range from 7143–65643 in macroalgal carbonates to 107–329 in scleractinian corals (Holmden et al., 2016; Pereira et al., 2016) and are higher than inorganic precipitation experiments (Tang et al., 2007; Rodler et al., 2015) in which $D_{\mathrm{Cr(VI)}}$ values range from approximately 0.1 to 3.4. Cultures of foraminifera under controlled conditions allow for a more accurate determination of the distribution coefficient in foraminifera whilst ruling out any post-depositional enrichment in Cr and any effects caused by the heterogeneity of Cr in seawater (Bonnand et al., 2013; Scheiderich et al., 2015; Paulukat et al., 2015; Economou-Eliopoulos et al., 2016; Paulukat et al., 2016; Pereira et al., 2016; Holmden et al., 2016).

Another critical factor in applying the Cr proxy to the fossil record is the lack of understanding of where in a foraminiferal test the Cr resides. Wang et al. (2017) concluded that <14% of Cr is adsorbed to clay particles and that the remaining Cr is in the carbonate in sedimentary foraminifera. However, Holmden et al. (2016) raise the issue that it is unclear whether uptake of Cr into carbonates takes place during precipitation or after deposition in the sediment. A recent study confirms that the primary marine Cr in marine biogenic carbonates signal may be diagenetically overprinted (Farkaš et al., 2018).

Here we seek to address the above-mentioned open questions to determine the faithfulness of Cr in foraminifera as a proxy for oxygen concentration, as well as its potential and limitations. First, we assess the distribution of Cr across foraminiferal test walls at high spatial resolution using laser ablation multi-collector ICP-MS (LA-MC-ICP-MS) and nanoscale SIMS (NanoSIMS) to determine the location of the Cr in the foraminiferal carbonate. We cultured benthic foraminifera to better constrain the distribution coefficient for Cr into foraminiferal calcite. We compared Cr concentrations between core-top, sediment trap, plankton net, and cultured samples to improve our understanding of the modes of Cr uptake into foraminifera. Finally, we assessed potential growth rate impacts by analysing a range of different mono-specific size classes and surface area to volume ratios to address post-depositional effects on Cr isotopic composition depending on particle sizes.

2. Material and analytical methods

2.1. Material

Foraminiferal specimens from four different sample types were used for this study: core-tops, plankton nets, sediment traps, and growth cultures (Table 1). Cultures were performed on benthic foraminifera *Amphistegina spp.* from Israel, and planktic *O. universa* and *G. ruber* from the Caribbean (Allen et al., 2016; Holland et al., 2017). *Amphistegina lobifera* specimens were collected from several sites along the Mediterranean coast of Israel (Nahsholim and Tel Shikhmona) and *Amphistegina spp.* were collected from the Red Sea coast of Israel (Eilat). Seawater for the culture medium of these benthic foraminifera was collected in cubitainers from Tel Shikhmona (Mediterranean Sea).

The planktic foraminifera *T. sacculifer* and *O. universa* were picked from core-tops SO456 and SO488 from the NW Australian margin. *T. sacculifer* and *G. ruber* were picked from core-top GeoB3915 located off the North-Brazilian coast. The planktic foraminifera *O. universa*, *G. menardii*, *G. ruber*, *G. truncatulinoides* and a mix of benthic foraminifera were picked from core-top samples from the Caribbean (Karibik; Caromel et al., 2014) and North Atlantic (T86-15S; Troelstra et al., 1987).

Sediment trap samples from off the coast of Cape Blanc in Mauretania (CB14) were picked for specimens of the planktic *G. truncatulinoides* and *T. sacculifer*. Specimens of *T. sacculifer* and *G. bulloides* were obtained from plankton net samples from the East China Sea (KT02-15B).

Table 1
Foraminiferal samples used for measuring Cr by LA-MC-ICP-MS. These include core-top samples, sediment trap samples, plankton net samples as well as cultured benthic foraminifera (this study) and planktic foraminifera (*O. universa* and *G. ruber;* Allen et al., 2016; Holland et al., 2017).

Sample	Type	Species	Laser spot size (μm)	Location
SO456 0-1 cm	Core-top	*T. sacculifer* *O. universa*	150 × 150	NW Australian margin
SO488 0-1 cm	Core-top	*T. sacculifer*	150 × 150	NW Australian margin
GeoB3915	Core-top	*T. sacculifer* *G. ruber*	150 × 150 85 × 85	Off Northern Brazil
CB14	Sediment trap	*G. truncatulinoides* *T. sacculifer*	85 × 85	Off Cape Blanc, Mauritania
KT02-15 B-2 10 m	Plankton net	*T. sacculifer*	130 × 130	East China Sea
KT02-15 B-2 50 m	Plankton net	*T. sacculifer*	130 × 130	
KT02-15 B-2 75 m	Plankton net	*T. sacculifer*	130 × 130	
KT02-15 B-2 100 m	Plankton net	*T. sacculifer*	130 × 130	
KT02-15 B-5	Plankton net	*G. bulloides*	130 × 130	
Amphistegina spp.	Culture	*Amphistegina spp.*	85 × 85	Israeli Red Sea and Mediterranean coast
O. universa	Culture	*O. universa*	130 × 130	Puerto Rico
G. ruber	Culture	*G. ruber*	130 × 130	Puerto Rico

2.2. Culturing *Amphistegina spp.* in chromium-doped seawater

To create the culture medium, LiCl (Merck EMSURE ACS Reag. Ph Eur) was added to 10 L of Mediterranean seawater to create a 500 μM Li solution. Lithium is used to distinguish newly formed foraminiferal chambers from chambers that formed prior to culturing, following Titelboim et al. (2017), where chambers with a high Li content formed during the culture experiments and low Li concentrations were formed before the experiments. Measurements on chambers with low Li concentrations were not considered in our partitioning studies. The Li-doped seawater was then divided into acid-cleaned 2 L HDPE bottles. Three 2 L aliquots were doped with 280 nmol, 560 nmol, and 840 nmol Cr from a chromate standard (Sigma-Aldrich TraceCERT 1000 mg/L chromate in water), respectively. This resulted in seawater with Cr concentrations of 2.75, 5.66, 6.73, and 8.39 nM, respectively. Two litres of seawater undoped with Cr served as a control on the experiment. Live specimens of *Amphistegina spp*. from Israel were picked, cleaned with a brush, and checked for activity. Twenty specimens were transferred to a sealable glass beaker containing the culturing medium with appropriate Cr concentration. All culture incubations were replicated. The foraminifera from the Mediterranean and Red Sea were kept separate. The seawater was refreshed once every week, and all experiments were performed at a temperature of 26 °C. Oxygen levels were monitored by Winkler titrations and with a PreSens Pst3 Oxygen Dipping Probe throughout the one month of culturing. The oxygen concentrations in the 1× [Cr] seawater for Mediterranean foraminifera were 171.3 and 172 μM at the beginning of the experiment measured by Winkler titration and dipping probe, respectively. The initial oxygen concentration in the 1× [Cr] seawater for Red Sea foraminifera measured by dipping probe was 155 μM. After the experiment, the specimens were cleaned and mounted whole onto carbon tape for LA-MC-ICP-MS analyses at the University of Cambridge, as described below (section 2.3).

One litre of the Li-doped seawater and three 100 mL aliquots of the Li and Cr-doped seawater were filtered and immediately acidified. An additional 1 L of Li-doped seawater and three 100 mL aliquots of Li and Cr-doped seawater were filtered but not acidified until the end of the experiment to track any potential changes in Cr content in the culture medium. The undoped seawater was analysed by ThermoFisher Scientific Neptune MC-ICP-MS at the National Oceanography Centre in Southampton following Goring-Harford et al. (2018). Doped seawater was analysed by ThermoFinnigan Element ICP-MS at the University of Bristol. Doped seawater was diluted in 2% HNO_3 by 4000 times. Synthetic standards containing Cr and other trace elements at a range of concentrations were used for calibration.

It is necessary to maintain tightly regulated Eh-pH levels to maintain a high concentration of dissolved Cr (Bonnand et al., 2013), which is difficult in a laboratory environment given the presence of living organisms in a relatively small volume of water and their symbiont activity and their own CO_2 flux. Therefore, to be confident about our D_{Cr} we measured final Cr concentrations in the culture medium, which ranged from 2.75 to 8.39 nM. This is less than expected given the amount of chromate solution that was added to the seawater and implies that we were either not able to maintain the stable Eh-pH levels required to prevent precipitation of Cr (Bonnand et al., 2013) or that there was Cr loss due to adsorption to vial walls. Our incubations fall within the range of natural seawater, with concentrations of ~1.2–9.5 nM (e.g. Scheiderich et al., 2015; Paulukat et al., 2016) and given the uncertainties in the rate of loss of Cr our D_{Cr} is an upper estimate. Higher Cr concentrations in the culture medium would result in even lower distribution coefficient values and, therefore, would further underscore our findings of low D_{Cr} in living larger benthic foraminifera.

2.3. Laser Ablation-MC-ICP-MS of foraminifera

Single species foraminiferal tests were picked from core-top, sediment trap, plankton net and cultured samples. The tests were cleaned by ultrasonication following Sadekov et al. (2008). The last three chambers of each test were removed using a surgical scalpel, resulting in 8-21 test fragments per analysis. These chamber fragments were mounted concave-side (inner surface) up on black carbon tape. The cultured *Amphistegina* were mounted whole and were analysed 10–21 times per culture set. High-resolution LA-MC-ICP-MS analyses were performed at the Department of Earth Sciences at the University of Cambridge and the School of Earth Sciences at the University of Western Australia using a pulsed Analyte G2 Excimer Laser (Teledyne Photon Machines Inc.; $\lambda =$ 193 nm) connected to a ThermoFisher Scientific Neptune Plus MC-ICP-MS. An MC-ICP-MS with a jet interface and in high-resolution mode was used to increase sensitivity and remove interferences.

Samples were ablated from the inner surface to the outer surface of the foraminiferal test along with the standards NIST SRM glasses 612 and 614, and a coral, JCp-1. The reproducibility of chromium concentrations for NIST SRM 612 was 36.45 ± 0.19 ppm (2SE), 0.91 ± 0.01 ppm (2SE) for NIST SRM 614, and 0.04 ± 0.004 ppm (2SE) for JCp-1. Our values are close to published Cr concentrations of 36.4 ± 1.5 ppm (2SE) for NIST SRM 612, 1.19 ± 0.12 ppm (2SE) for NIST SRM 614 and 0.14 ± 0.015 ppm (2SE) for JCp-1 (Inoue et al., 2004; Jochum et al., 2011). The species ^{48}Ca, ^{50}Cr, ^{51}V, ^{52}Cr, ^{53}Cr, ^{55}Mn and ^{56}Fe were measured in planktic foraminifera (core-top, sediment trap, plankton net, culture samples) as well as cultured benthic foraminifera (Table 1). Data reduction of depth profiles removed the mean background intensity and standardised data to ^{48}Ca and NIST SRM 612 and 614 (Sadekov et al., 2008). Each depth profile took 10–24 s to measure, depending on the thickness of the test, and each single measurement within a depth profile was made over an average of 0.5 s. Laser spot sizes varied between 85 to 150 µm to best fit the test fragments (Table 1) and were standardised against standards using the same spot size. Prior to analysis the test fragments were pre-ablated to remove the outer 1 µm of the surface for additional cleaning purposes (Sadekov et al., 2008).

2.4. NanoSIMS imaging of planktic foraminiferal test walls

Cleaned foraminifera tests were placed on parafilm, embedded in resin (Araldite 2020) discs of 1 cm diameter and 5 mm height, and cured at 20 °C for 48 hr. The discs were polished using silicon carbide wet grinding paper with decreasing coarseness (HERMES, WS Flex 18C, 230 mm, P 800 and ATM, SIC wet grinding paper, grain 4000) to expose cross sections perpendicular to the test walls of the embedded foraminifera. When the exposure was sufficient, as determined by light microscopy, final polishing was carried out using agglomerated alpha alumina powder (Struers AP-A powder, grain size 0.3 µm) and SiO_2 powder (Logitech SF1 Polishing Suspension, grain size 0.035 µm). Polished samples were subsequently cleaned in ethanol in an ultrasonic bath for 5 seconds and coated with a 20 nm Au layer using a sputter coater (JEOL JFC-2300HR high resolution fine coater, JEOL FC-TM20 thickness controller). For orientation purposes the samples were imaged with a table-top SEM (JEOL JCM-6000PLUS NeoScope Benchtop SEM).

Nanoscale secondary ion mass spectrometry was performed with a nanoSIMS 50L instrument (Cameca) operated at Utrecht University. Using an element standard (SPI Supplies, 02757-AB 59 Metals & Minerals Standard), magnetic field and exact positions of the electron multiplier detectors were adjusted to enable detection of secondary ions $^{24}Mg^+$, $^{44}Ca^+$, $^{52}Cr^+$, $^{55}Mn^+$ and $^{56}Fe^+$. The correct tuning for ^{52}Cr was verified by initially measuring ^{50}Cr from both the SPI standard and the sample, which gave the correct $^{50}Cr/^{52}Cr$ atom ratio of 0.052. Before each measurement, the sample area of interest (square of 40–70 µm in size) was pre-sputtered with a primary O^- ion beam of 280 pA (using diaphragms D0-2 and D1-1) for 8–10 min until the secondary ion count rates stabilised. Subsequently, secondary ion images were acquired by rastering the primary O^- ion beam of about 50 pA over the sample surface (square of 30–45 µm in size) and detecting the ions with a dwelling time of 2–5 ms/pixel and with the diaphragm and slit settings of D0-2, D1-3, ES-3, AS-2 and EnS-1. For these settings, the nominal size of the primary O^- ion beam was 400-600 nm. Due to the very low count rates of the trace elements Cr, Mn and Fe, measurements took between 5 and 14 hr per sample area. Overall, five wall sections from a Holocene *T. sacculifer* from the Karibik core-top sample (Caromel et al., 2014; section 2.1) were imaged. Processing and analysis of the nanoSIMS data was done using Look@nanoSIMS, as previously described by Polerecky et al. (2012).

2.5. Chromium analysis of planktic foraminifera by (MC-)ICP-MS

Approximately 0.1 g of multiple planktic foraminiferal species (*O. universa*, *G. menardii*, *G. ruber*, *G. truncatulinoides*) were picked from core-top samples from the Caribbean (Karibik; Caromel et al., 2014) and North Atlantic (T86-15S; Troelstra et al., 1987) in different size fractions (>500 µm and 250–500 µm). Samples obtained for Cr isotope analysis were cleaned by gently cracking open the foraminiferal tests followed by rinsing with MilliQ water and methanol to remove clay particles, and with alkali buffered H_2O_2 to remove organic matter (Barker et al., 2003). Baturin and Dubinchuk (2011) reported 8-40 ppm Cr in ferromanganese nodules, which suggests there is a small contribution of authigenic Cr in ferromanganese coatings on the outside of the foraminiferal shell to the overall Cr content in foraminifera. On average, ferromanganese coatings contribute 1 ppm Mn to the total Mn content in our foraminiferal samples (Supplementary Material). Assuming an average Mn concentration of 15.2% in ferromanganese nodules (Baturin and Dubinchuk, 2011), ferromanganese coatings on foraminifera contribute up to 0.0003 ppm Cr, which is negligible compared to the overall foraminiferal Cr concentration in our samples. Acid leaches with 0.001 M nitric acid and reductive steps with a citric acid, ammonia and hydrazine mixture also introduced non-foraminiferal Cr (Supplementary Material). We therefore decided not to remove these to preserve as much of the sample as possible for analysis. The samples were then dissolved in 0.5 M acetic acid. An aliquot of 0.01 g of sample was dried down to incipient dryness and re-dissolved and diluted in 2% HNO_3 to produce a 100 ppm Ca solution. Matrix-matched synthetic standards doped with 100 ppm Ca and containing trace elements at a range of concentrations were used as calibration. Chromium and rare earth elements and Yttrium (REE-Y) concentrations were measured in O_2 collision mode on an Agilent 7500s ICP-QQQ-MS at the School of Environment, Earth and Ecosystem Sciences at the Open University. Chromium concentrations were reproducible within ∼2% and REE-Y were reproducible within ∼9% using replicate measurements of dolomite standard reference JDo-1. REE-Y measurements were made for sequential leaching experiments to monitor the presence of a ferromanganese coating as REEs reside mostly in the coating (Palmer, 1985). Chromium isotopes were measured on a ThermoFisher Scientific Neptune MC-ICP-MS at the University of Bristol using a ^{50}Cr-^{54}Cr double-spike technique following Bonnand et al. (2011). The contribution of the blank is negligible, with a total procedural blank for Cr of ∼0.2 ng. The standard JDo-1 was subjected to the same cation exchange chromatography protocol as the samples and the average value of JDo-1 was $\delta^{53}Cr = 1.716 \pm 0.069‰$ (2σ, $n = 10$). The external reproducibility of 50 ng of NBS 979 was $\delta^{53}Cr = 0.049 \pm 0.072‰$ (2σ, $n = 30$). Our values for JDo-1 and NBS979 are within uncertainty of previously published values (Bonnand et al., 2011).

3. Results

3.1. Chromium uptake by benthic foraminifera

Amphistegina spp. and *A. lessonii* Cr concentrations increase with rising Cr concentrations in the culture medium (Fig. 1). The outliers in the dataset have larger errors than the data falling within clusters, which potentially could have been caused by contamination. Chromium concentrations of bulk single foraminifera were obtained by averaging LA-ICP-MS profiles. Average Cr concentrations in *Amphistegina* strongly correlate with total Cr concentrations in the culture medium ($R^2 = 0.78$; $p = 0.002$; Fig. 2), showing that availability of Cr exerts a direct control on uptake by foraminifera. The distribution coefficient was 250 ± 43, as determined from the slope of a linear regression between the Cr con-

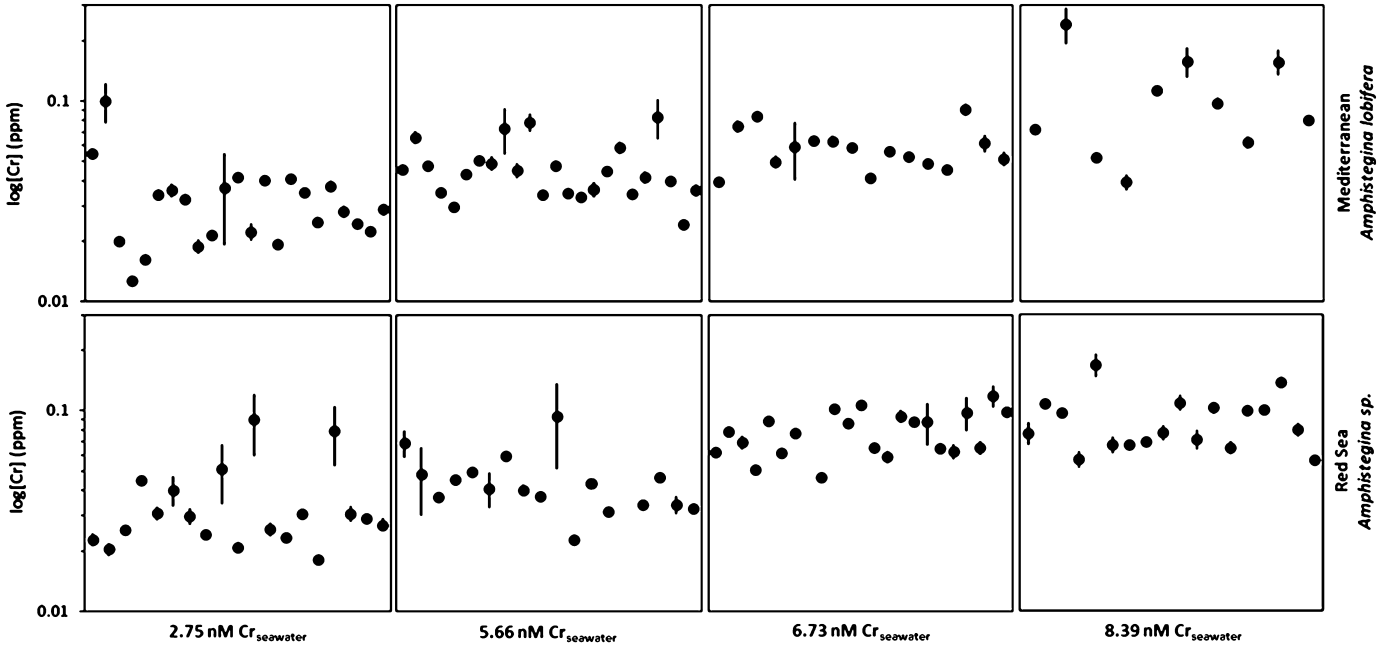

Fig. 1. The Cr concentrations of single foraminifera in cultures of the larger benthic foraminifer *Amphistegina spp*. measured by LA-MC-ICP-MS. Culturing conditions were under natural seawater (2.75 nM Cr), and seawater spiked with Cr to reach final concentrations of 5.66 nM, 6.73 nM, and 8.39 nM. Chromium concentrations in the foraminifers increase with increasing dissolved Cr concentrations in the water. Where error bars are not visible, the analytical uncertainties are smaller than the size of the data point.

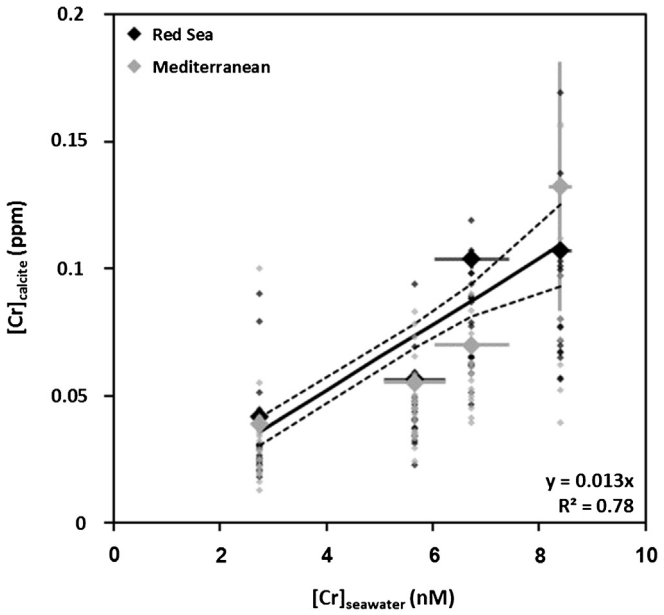

Fig. 2. Specimens of the foraminiferal species *Amphistegina spp*. from the Red Sea and *A. lobifera* from the Mediterranean were cultured in natural and chromate-spiked Mediterranean seawater with concentrations between 2.75 and 8.39 nM Cr. Large black diamonds represent average Cr concentrations and small black diamonds are all Cr concentration measurements in the *Amphistegina spp*. cultures from the Red Sea, whereas large grey diamonds are average Cr concentrations and small grey diamonds are all Cr concentration measurements in the *A. lobifera* cultures from the Mediterranean. The solid black line is the linear regression of the data, forced through the origin, and has a slope of 0.013 ± 0.006 (2SE) with $p = 0.0015$ and $R^2 = 0.78$. The dashed lines outline the 95% confidence interval of all the data around the slope. The correlation between the average total Cr concentration in seawater and in the foraminiferal test results in a distribution coefficient of $D_{Cr} = 250 \pm 43$ (2SE) after unit conversion of $[Cr]_{seawater}$ into ppm. Where error bars are not visible, the analytical errors are smaller than the size of the data point.

centrations in the test walls and in the culture medium. Undoped Mediterranean coastal seawater at Nachsholim (Israel) has a δ^{53}Cr value of 1.14 ± 0.06‰ (2SD) and Cr concentrations of 2.75 nM. Some of the scatter is likely due to decreasing Cr concentrations in the culture medium.

3.2. Spatial distribution and concentrations of chromium in planktic foraminifera

The distribution of Cr in core-top foraminifera, determined by LA-MC-ICP-MS, ranges from homogeneous to strong enrichments in Cr towards the rim of the test in core-top foraminifera (Fig. 3; Supplementary Material). The total range of chromium concentrations in foraminifera reveal differences of up to two orders of magnitude. On average, core-top foraminifera have elevated Cr levels (~0.82 ppm) compared to ~0.09 ppm in foraminifera that come from sediment traps, plankton nets, and cultures (Fig. 4).

The relatively homogeneous distribution of Cr through the test shown by laser ablation data is confirmed by NanoSIMS analysis of a Caribbean core-top *T. sacculifer*. However, the higher spatial resolution of the NanoSIMS reveals elevated Cr concentrations in prominent Mg-rich bands that align with the primary organic sheet (POS), as identified by grooves in the calcite (Fig. 5). While the Cr-rich bands were always co-localised with elevated Mg, Mn and Fe concentrations, only some of the Mg and Mn bands had elevated Cr concentrations (Fig. 5).

The LA-MC-ICP-MS data reveal that when Cr is plotted against Fe/Ca and Mn/Ca ratios there are two distinct populations, with non-sedimentary foraminifera generally plotting at lower Fe/Ca and Mn/Ca ratios than the core-top foraminifera (Fig. 6a and 6b). In both populations, Cr concentrations correlate strongly with Fe/Ca of the foraminifera ($R^2 = 0.85$ and 0.95; $p < 0.00001$), suggesting a common uptake pathway into the foraminiferal test. In contrast, there is only a strong correlation between Cr and Mn/Ca for the non-sedimentary foraminifera. The plots also reveal that some core-top foraminifera plot close to the non-sedimentary data, and fall on a distinct trend between the two populations. In general, the foraminifera with both high Cr concentrations and high Fe concentrations have low Mn concentrations (Fig. 6c). These correlations are confirmed by the NanoSIMS analysis of core-top foraminifera (Fig. 5) and shows that also Cr and Mn/Ca strongly correlate within a single *T. sacculifer* specimen.

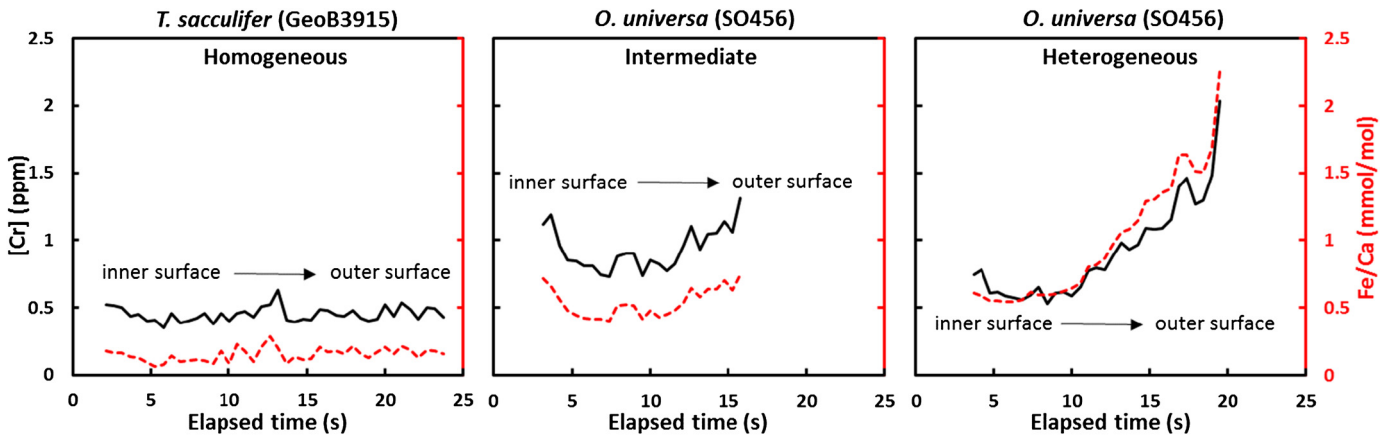

Fig. 3. Three laser ablation (LA-MC-ICP-MS) profiles of Cr concentrations, and Fe/Ca through planktic foraminiferal calcite (*T. sacculifer* and *O. universa*) in two core-top samples (GeoB3915 and SO456). These are representative of the Cr profiles in foraminifera, displaying distributions ranging from homogeneity throughout the test to strong enrichment at the rim of the test. An overview of all planktic foraminiferal Cr concentration profiles obtained through LA-MC-ICP-MS can be found in the Supplementary Material.

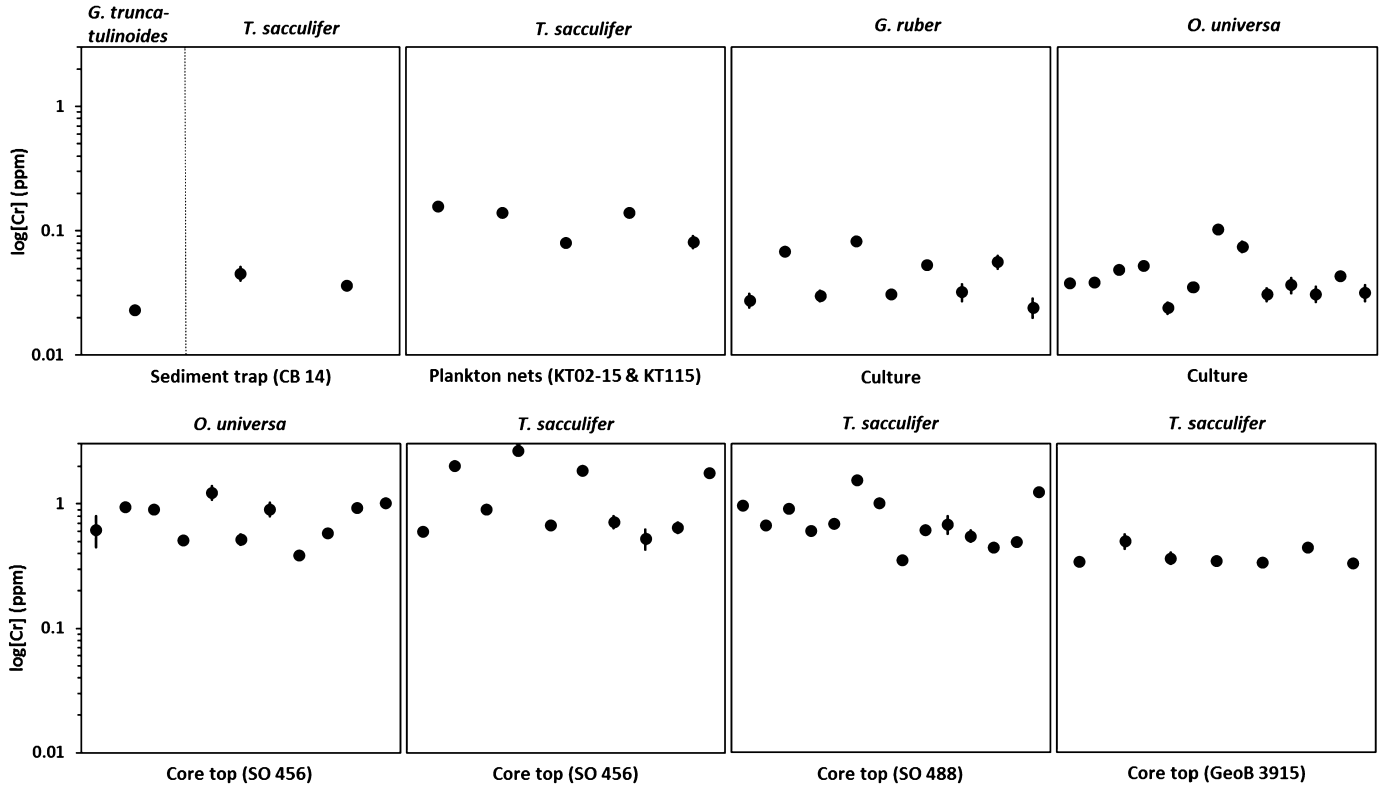

Fig. 4. Chromium concentrations of individual planktic foraminifera measured by LA-MC-ICP-MS in core-top, sediment trap, plankton net, and culture samples. Chromium concentrations are higher in core-top samples than in non-sedimentary (sediment trap, plankton net, cultured) foraminifera. Where error bars are not visible, the analytical uncertainties are smaller than the size of the data point.

3.3. Chromium isotopic composition of core-top planktic foraminifera

Chromium concentrations in core-top samples from the Caribbean are higher (0.15–0.38 ppm) compared to those from the North Atlantic (0.06–0.08 ppm) while δ^{53}Cr was ~0.4‰ lower. Specimens from the >500 µm fraction have δ^{53}Cr values 0.3–0.5‰ higher than those from the 250–500 µm size fractions in both the Caribbean and North Atlantic (Fig. 7). Offsets in Cr concentrations associated with size fractions of foraminifera are less clear. While the smaller foraminifera, and particularly *G. ruber*, may have higher Cr concentrations in the Caribbean, this is not the case for foraminifera from the North Atlantic where Cr concentration are within analytical uncertainty for all species analysed. There is a lack of species-specific fractionation and differences in isotopic composition are therefore not affected by different foraminiferal habitats or biology.

4. Discussion

Our new data allow for an assessment of the utilisation of Cr and its isotopes in foraminifera as a palaeoproxy for oceanic redox conditions. Specifically, we can assess the uptake mechanism of Cr, its distribution within foraminiferal calcite, and whether there is any fractionation of Cr isotopes by foraminifera.

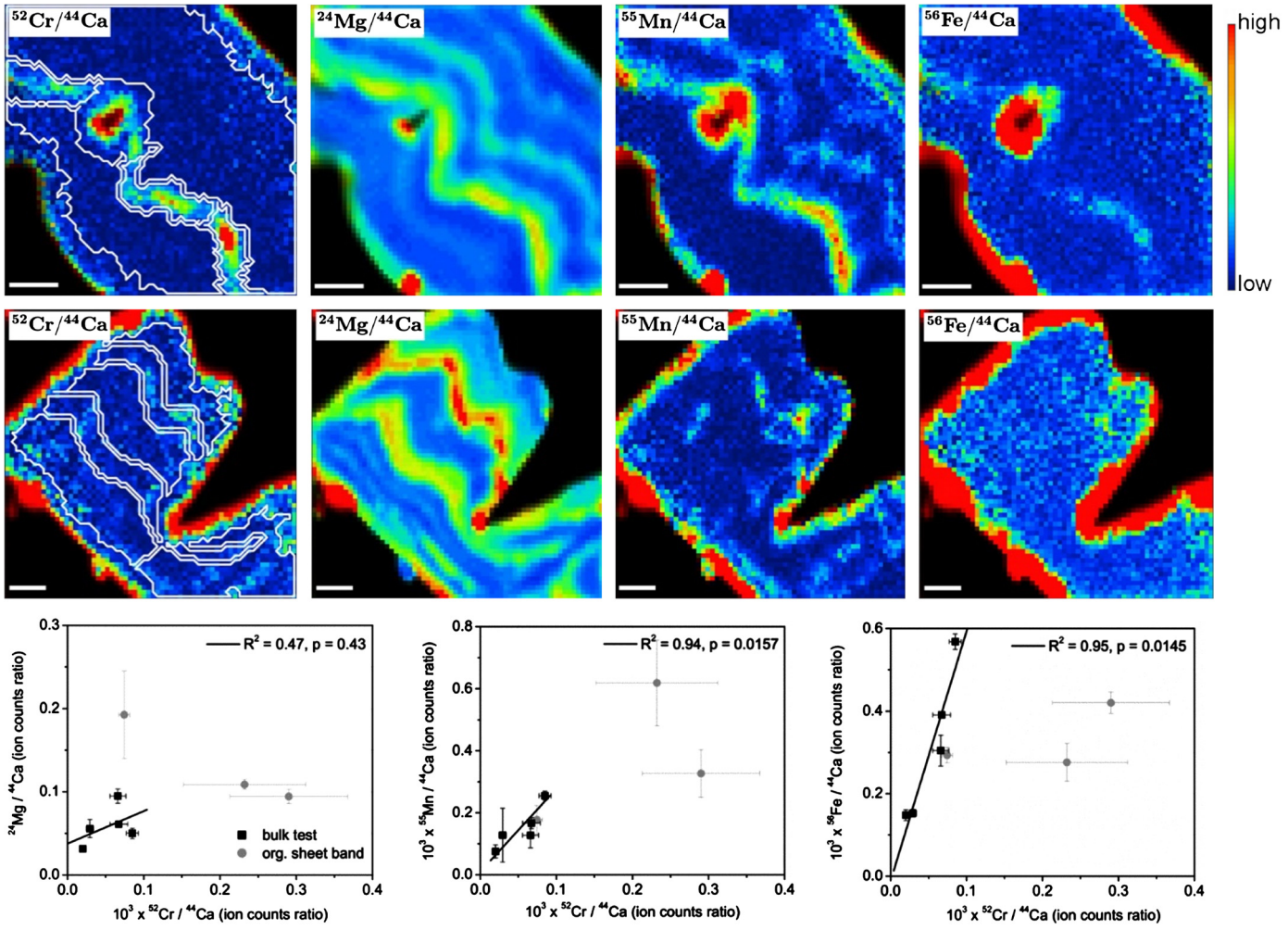

Fig. 5. NanoSIMS images and analysis of core-top *T. sacculifer* specimens from the Caribbean (Caromel et al., 2014). NanoSIMS image panels show ^{52}Cr, ^{24}Mg, ^{55}Mn, and ^{56}Fe to ^{44}Ca ratios within the test walls. All trace elements were enriched in a layer associated with the POS. The apparent increase in Cr/Ca ratios at the rim of the foraminiferal tests is an analytical artefact of the transition from higher Cr and lower Ca counts in the resin to lower Cr and higher Ca counts in the test, caused by the limited spatial resolution of the nanoSIMS beam used in this study (400–600 nm). This artefact occurs for all element/Ca ratios. Regions of interest (ROIs), indicated by the white outlines in the left panels, were drawn to calculate average Cr/Ca, Mn/Ca and Fe/Ca ratios in the 'bulk' test and the Cr-rich bands. ROIs were divided into 3–4 approximately equal parts to estimate variability within an ROI. Within the bulk tests, the correlations between Cr/Ca, Mn/Ca and Fe/Ca are significant, whereas there is no apparent correlation with Mg/Ca. The Cr-rich bands associated with the POS do not follow the trends defined by the bulk test.

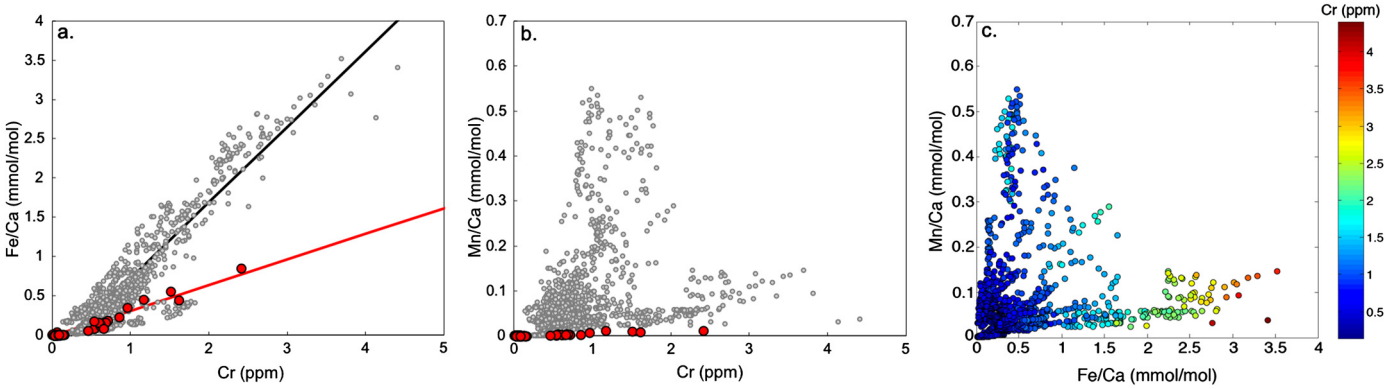

Fig. 6. a. Cross-plot of average Cr concentrations and Fe/Ca obtained by LA-MC-ICP-MS in single foraminifera. Core-top samples are in grey and non-sedimentary foraminifera are in red. There are two populations with distinct trends in the core-top samples of which one overlaps with the non-sedimentary foraminifera. **b.** Cross-plot of average Cr concentrations and Mn/Ca obtained by LA-MC-ICP-MS of single foraminifera. Core-top samples are in grey and non-sedimentary foraminifera in red. There is no trend in the core-top samples. There is, however, a significant trend within non-sedimentary foraminifera. **c.** There is no correlation between Mn/Ca and Fe/Ca. Chromium is present in high concentrations in foraminifera with high Fe concentrations. Samples with a high Fe and Cr content have lower Mn concentrations. (For interpretation of the colours in the figure(s), the reader is referred to the web version of this article.)

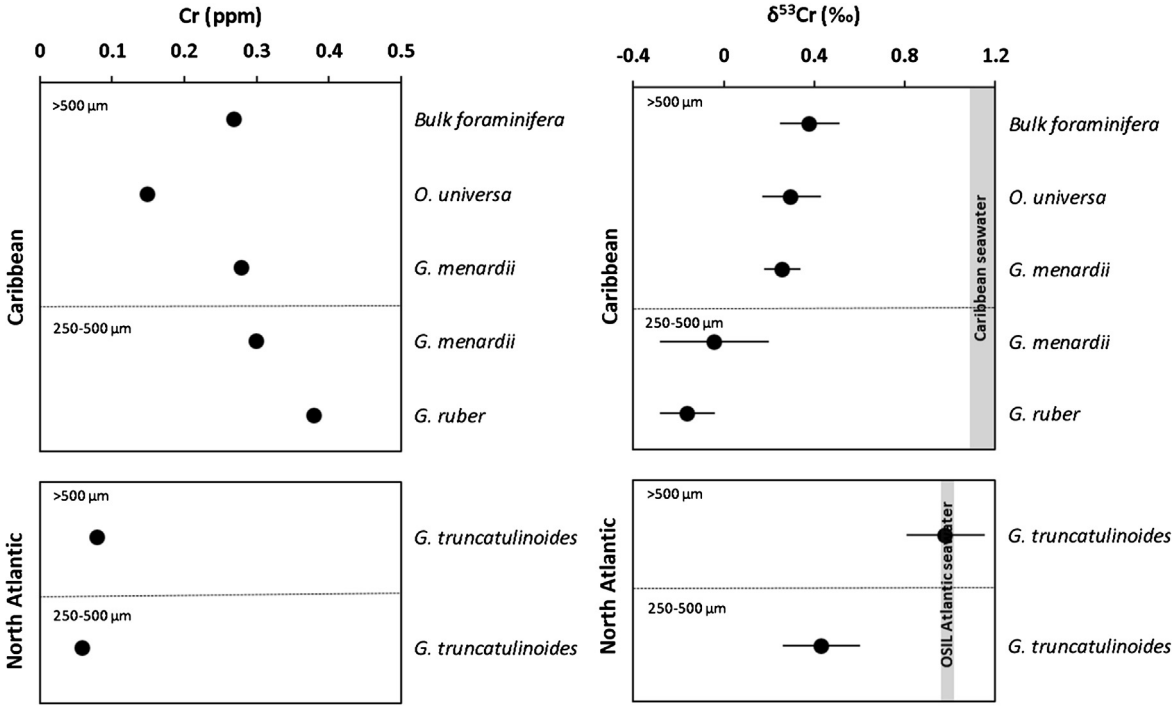

Fig. 7. The Cr content (left panels) and δ^{53}Cr composition (right panels) of foraminifera of different sizes from the Caribbean and North Atlantic (T86-15S). There are no vital effects between different species of foraminifera of the same size fraction. There is, however, an isotopic offset between size fractions. Seawater δ^{53}Cr values are from Scheiderich et al. (2015) and Holmden et al. (2016). Where error bars are not visible, the analytical uncertainties are smaller than the size of the data point.

4.1. Chromium uptake by benthic and planktic foraminifera

The distribution coefficients for the larger benthic foraminifera *Amphistegina spp.* ($D_{Cr} = 250 \pm 43$) are comparable to scleractinian corals ($D_{Cr} = 107–329$; Pereira et al., 2016), despite the difference in crystal structure between aragonite and calcite (Soldati et al., 2016). Our data also approach the lower end of previous estimates for planktic foraminiferal distribution coefficients from core-top samples (Wang et al., 2017), molluscs (Farkaš et al., 2018), and bivalves (Frei et al., 2018), but are significantly lower than distribution coefficients for sedimentary macroalgal carbonates with a D_{Cr} of 7143–65643 (Holmden et al., 2016). The D_{Cr} estimates based on core-top foraminifera are generally substantially higher and range between 303 and 4000 (Wang et al., 2017). However, these foraminiferal core-top calibrations are based on average seawater Cr concentrations from the Atlantic and Pacific Oceans (Wang et al., 2017) and given the heterogeneity of modern surface seawater (e.g. Goring-Harford et al., 2018) need to be approached with caution. There is a notable difference in the range of distribution coefficients associated with cultured foraminifera ($D_{Cr} = 107–329$) and sedimentary carbonate ($D_{Cr} = 303–65643$).

On average, core-top specimens have an order of magnitude higher concentrations (0.82 ppm) than non-sedimentary foraminifera, which have 0.09 ppm Cr (Fig. 4). The laser ablation data are not influenced by coatings on the outside of the test and remnants of clay in pores of the core-top foraminifera would not have caused such an increase. Therefore, our laser ablation measurements and culture experiments imply that most Cr (~89%) in foraminifera is likely to be derived through some post-depositional processes, as suggested by Holmden et al. (2016). This is confirmed by a high Cr concentration of 1.16 ppm in a mix of core-top benthic foraminifera. Concentrations similar to those of non-sedimentary foraminifera were also found in our culturing experiments and in non-sedimentary aragonitic scleractinian corals (0.04–0.07 ppm; Pereira et al., 2016). These data suggest that at seawater Cr concentrations of 2–10 nM (e.g. Scheiderich et al., 2015; Paulukat et al., 2016) both forms of carbonate incorporate a limited amount of Cr. However, our culturing experiments suggest that incorporation is controlled by a partition coefficient, so that primary Cr concentrations in foraminifera increase with increasing seawater concentrations.

4.2. Spatial distribution of chromium in planktic foraminifera

Chromium is present across the whole test (Fig. 3). The enrichment in chromium near the rims of some of the tests (Fig. 3) indicates a potential penetration into the test from the bottom and pore water in which they reside, supporting post-depositional processes as a main source of Cr into the test (Fig. 4). The considerable spatial variability in some laser ablation depth profiles warranted increased spatial resolution analyses by NanoSIMS. NanoSIMS imagery showed increased Cr counts in the most prominent cyclical Mg-rich bands (Fig. 5). These bands are associated with chamber formation and appear to be light-triggered (Fehrenbacher et al., 2017). While NanoSIMS is extremely sensitive to surface topography, and could artificially produce enriched layers caused by cracks in the surface, we were extremely careful during sample preparation not to damage the surface. The initial inner calcite layer makes up a small fraction of the total foraminiferal shell compared to the rest of the ontogenetic calcite and potential gametogenic calcite, and is thought to be enriched in trace elements (Eggins et al., 2003; Erez, 2003). The fact that not all Mg-rich bands were accompanied by increased Cr counts was potentially due to the relatively low Cr concentrations (<1 ppm; Fig. 7) combined with the sensitivity of the NanoSIMS. The enrichment of Cr in Mg-rich bands was not detected by laser ablation techniques, likely due to the lower spatial resolution of the laser (1–4 µm) compared to the NanoSIMS (400–600 nm), the former averaging out the distinct Cr-rich layers within the bulk calcite during analysis.

There are two possible interpretations for these higher Cr concentrations. Firstly, the higher concentration could be post-depositional Cr overprints. Interestingly, the Cr-rich bands aligned

with discontinuities in the calcite that are remnants of the position of the primary organic sheets (POS) (Fig. 5). This suggests Cr in core-top foraminifera may have penetrated the tests through cracks which acted as access points for pore waters and thus provides an alternative pathway for Cr (and likely other elements) to diffuse through the test. Erez (2003) hypothesised that a potential initial calcification mechanism may be through endoplasmatic granules or organic matrix, which would lead to higher trace element concentrations. Therefore, an alternative hypothesis for the alignment of Cr-rich bands with regions associated with the primary organic sheet is an enrichment of Cr in the inner calcite layer. Jacob et al. (2017) suggest that the initial stages of foraminiferal biomineralisation occur via metastable carbonate phases such as vaterite, and potentially also amorphous calcium carbonate. Vaterite is fibrous and has nanopores, which likely contain organic material (Li et al., 2011; Jacob et al., 2017), increasing the potential of high Cr concentrations.

4.3. Source of Cr in the geological archive

Plots of Fe/Ca, Mn/Ca and Cr in core-top foraminifera obtained by laser ablation methods clearly demonstrate that these foraminifera fall into two separate populations: one with high Fe/Ca and Mn/Ca ratios and one that overlaps with non-sedimentary foraminifera from plankton tows, cultures and sediment traps (Fig. 6). Our data indicate that Cr is initially taken up by foraminifera upon precipitation of their carbonate shell, at low concentrations comparable to those observed in non-sedimentary samples. This signature is preserved in some core-top foraminifera but is often overprinted by exchange with bottom and pore waters after deposition in the sediment, which increases the Cr concentration. Core-top foraminifera with a high Cr content have high Fe and low Mn concentrations, which reinforces the observation that foraminiferal Cr is independent of Mn and may be influenced by oxyhydroxides low in Mn (Fig. 6c). Minerals common in the environment containing both Fe, Mn and Cr include Fe–Mn and Cr(III)–Fe(III) oxyhydroxides (Tang et al., 2010). The highest Cr and Fe contents in non-sedimentary foraminifera are found in the upwelling zone off the coast of Mauritania (Table 1), which receives large amounts of Fe and other metals from Saharan dust (e.g. Hatta et al., 2015). The strong correlation between Fe and Cr within non-sedimentary and core-top foraminiferal tests suggests that they have a similar pathway into the foraminiferal calcite. However, core-top foraminifera define two distinct populations; a high Cr concentration population that also have elevated Fe/Ca and Mn/Ca ratios and a population that is more similar to the non-sedimentary foraminifera with low Cr concentrations (Fig. 6), which suggests two episodes of Cr uptake. The strong correlation between Cr and Fe/Ca as well as Mn/Ca within a single core-top planktic foraminifer is visible in the NanoSIMS analysis (Fig. 5), and is indicative of the second episode related to post-depositional Cr incorporation. Chromium(III)–Fe(III) oxyhydroxides are a reaction product of Cr(VI) reduction by Fe(II) (Ellis et al., 2002). Iron and Mn bearing oxyhydroxides could influence foraminiferal δ^{53}Cr by the reduction of Cr(VI) to Cr(III) by Fe(II) and the oxidation of Cr(III) to Cr(VI) by Mn in pore and bottom waters (e.g. Schroeder and Lee, 1975; Døssing et al., 2011). A potential pathway for elevating Cr and Fe concentrations in pore and bottom waters is through solubilisation of Cr(III) and Fe(III) bound to Cr(III)–Fe(III) oxyhydroxides through oxidation by Mn or by ligand complexation (Saad et al., 2017). The reduction of Cr(VI) by Fe(II) would produce heavier δ^{53}Cr values in the remaining Cr(VI) pool, whereas the addition of isotopically light Cr(III) due to oxidation of Cr(III) by Mn would drive the Cr(VI) pool to lighter δ^{53}Cr values.

The post-depositional enrichment of Cr is substantially greater than the Cr uptake associated with the live phase, and therefore core-top and down-core foraminifera most likely carry a bottom and pore water Cr isotopic signature rather than a sea surface Cr isotopic value. The overlap between some low Mn-Fe core-top foraminifera and non-sedimentary specimens may provide a useful criterion for distinguishing foraminifera affected by post-depositional uptake of Cr into their tests.

4.4. Chromium isotopic composition of core-top planktic foraminifera

Given the impact of post-depositional processes on foraminiferal Cr concentrations the question arises as to how much the same processes alter the Cr isotopic composition of foraminifera. The absence of species-specific fractionation (Fig. 7) between foraminifera of the same size class indicates that the Cr isotopic composition in core-top foraminifera is not determined by biological processes, as we assessed specimens from different water depths and ecologies. This is in contrast to other isotope systems which are heavily influenced by biological processes (e.g. Schmidt et al., 2008). While *G. ruber* and *O. universa* live in the upper mixed layer and have symbionts which add to the foraminifer's control on changing the oxygen concentration around the test, *G. menardii* and *G. truncatulinoides* dwell without symbionts below the thermocline for a significant amount of time during calcification, and would therefore experience the lower oxygen concentrations of the deep chlorophyll maximum, at least for parts of their life (Hemleben et al., 1989).

Our foraminiferal Cr isotope data suggest that the size of core-top foraminifera influences the susceptibility of the test calcite to post-depositional exchange with Cr in pore and bottom waters. Larger foraminifera have δ^{53}Cr values closer to nearby reported relatively heavy seawater values, whereas smaller foraminifera have a lighter Cr isotopic composition and more closely resemble bulk silicate earth. We expect pore waters to be closer in δ^{53}Cr to bulk silicate earth values (-0.124‰; Schoenberg et al., 2008) due to the large quantities of isotopically light Cr(III) available for remobilisation in the sediment. The post-depositional addition of isotopically light Cr is possible through the oxidation of authigenic Cr(III) phases with light δ^{53}Cr values by Mn to Cr(VI) which can readily be incorporated in the carbonate. Although a second mechanism could be the solubilisation of Cr(III) through ligand complexing (Saad et al., 2017), it is not yet clear how these complexes can be incorporated into a carbonate lattice.

A potential abiotic control on the relationship between size and Cr is the change in surface area to volume ratio, an impact also seen in foraminiferal Mg (Schmidt et al., 2008). The inverse relationship between test diameter and δ^{53}Cr is associated with a higher surface area to volume ratios (A/V) in smaller specimens. As such, their calcite volume is more susceptible to alteration by post-depositional Cr enrichment via exchange with Cr in bottom and pore waters, as seen in other isotope systems such as B (e.g. Hönisch and Hemming, 2004; Ni et al., 2007). The addition of isotopically light Cr through these post-depositional processes would also provide an explanation for the apparent -0.46‰ fractionation in macroalgal sediments and surface seawater in the modern Caribbean Sea (Holmden et al., 2016). To assess this interpretation, A/V calculations were based on the test volume determined from the same samples by Caromel et al. (2014). Surface areas were calculated assuming a spherical shape for *O. universa* and *G. ruber*, a discoidal shape for *G. menardii* and a conical test for *G. truncatulinoides*. Our data illustrate that foraminifera record a similar isotopic offset between size fractions, even with widely differing shell shapes, pore volumes and thicknesses. Due to their shape, the discoidal *G. menardii* are more prone to changes in A/V than the spherical *O. universa*, globular *G. ruber*, and conical *G. truncatulinoides* (Fig. 8). These surface area approximations are a minimum estimate for *G. ruber*, which is highly porous and has an open

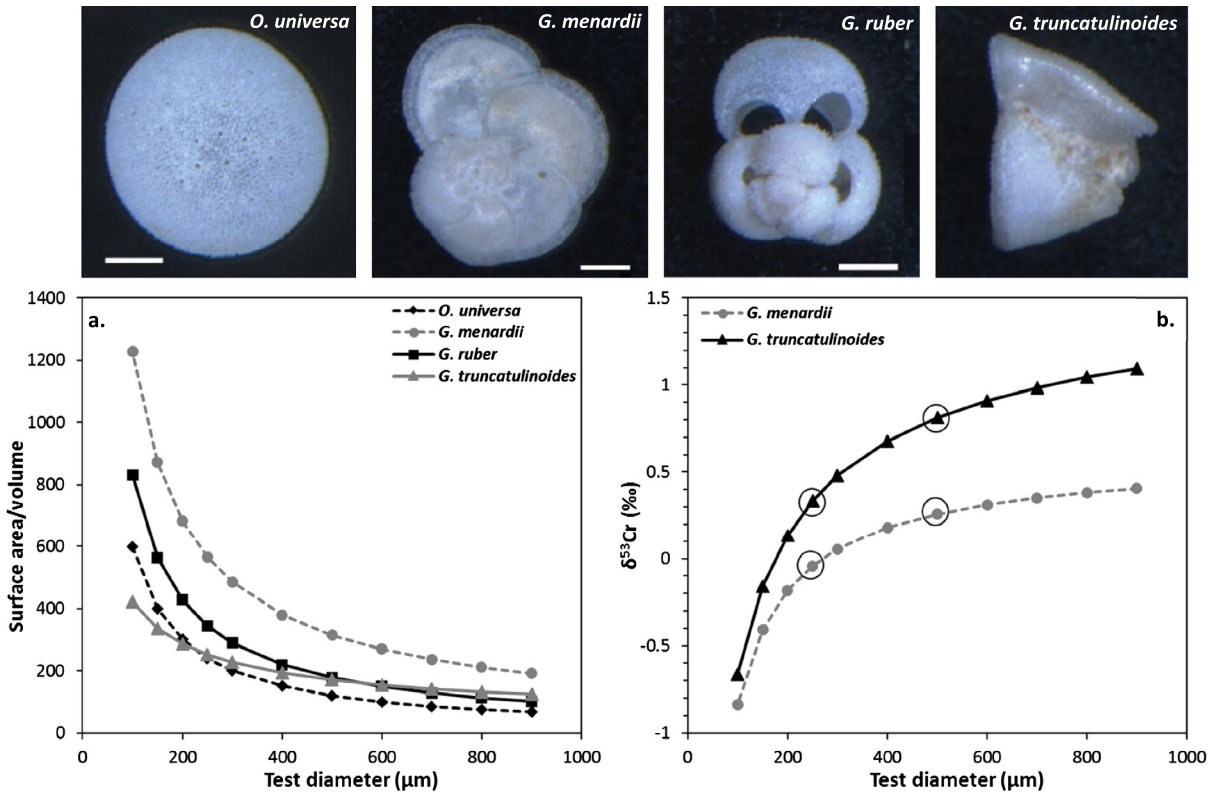

Fig. 8. a. Simulated surface area to volume (A/V) ratios based on volume – test diameter measurements by Caromel et al. (2014) show that A/V ratios in planktic foraminifera increase markedly in smaller size fractions (<500 µm). Smaller foraminifera are therefore more susceptible to diagenetic processes. **b.** A model of linear dependence of foraminiferal Cr isotopes on the A/V ratio shows that the largest changes in isotopic composition would occur at smaller test diameters. The original Cr isotope data on which the linear model is based are encircled. Microscope images of planktic foraminifera to illustrate the shapes of the foraminiferal used for modelling A/V ratios are from Caromel et al. (2014).

test structure and as such is more prone to overprinting. Both *G. menardii* and *G. truncatulinoides* have lower-Mg calcite and robust tests, and are therefore less susceptible to dissolution and post-depositional overprinting. Despite these differences in shape, all planktic foraminifera show a sharp change in slope in the A/V ratio between 250–300 µm. Foraminifera smaller than 250 µm are likely to record even larger isotopic offsets due to the increase of the A/V ratio with decreasing test size (Fig. 8). Assuming a linear dependence of the Cr isotopic composition of *G. menardii* and *G. truncatulinoides* on the A/V ratio (taken as the A/V ratio for the lowest end-member of the size fractions, i.e. 250 and 500 µm), the variability in foraminiferal Cr isotopes reported by Wang et al. (2017) can be explained by potential differences in the sizes of the foraminifera analysed (Fig. 8). The negative modelled δ^{53}Cr values for foraminifera smaller than approximately 250 µm are similar to the δ^{53}Cr composition of ferromanganese crusts, which ranges from −0.85 to −0.15‰ (Wei et al., 2018), while modelled foraminiferal δ^{53}Cr compositions for larger specimens are more similar to seawater δ^{53}Cr (Fig. 8; Bonnand et al., 2013; Scheiderich et al., 2015; Paulukat et al., 2016; Goring-Harford et al., 2018). Foraminifera larger than 500 µm are therefore more likely to record a primary Cr signature, with a maximum isotopic offset of 0.1–0.2‰ (Fig. 8).

5. Conclusions

Both laser ablation and NanoSIMS analyses show that Cr is distributed across the whole foraminiferal shell. Multiple analyses of foraminiferal Cr suggest that most Cr in foraminifera is added after burial in the sediment. There is no interspecies isotope fractionation, which is consistent with a mostly post-depositional origin of Cr in foraminifera. Sedimentary foraminifera have, on average, an order of magnitude more Cr than foraminifera collected before deposition. Cultured benthic foraminifers have a D_{Cr} of up to 250 ± 43, which is comparable with scleractinian corals, and Cr concentrations ranging between 0.04 to 0.13 ppm under natural seawater Cr concentrations. Given uncertainties in our experiments, the D_{Cr} is the upper boundary of possible values. Overall, foraminiferal Cr (and Cr in carbonates in general) therefore does not record the sea surface Cr composition. Instead, it records the Cr composition of bottom and pore waters at the time of deposition. This is corroborated by two distinct populations in Cr to Fe/Ca and Mn/Ca cross-plots, which also suggest a post-depositional overprint in core-top foraminifera. However, this study suggests that Fe and Mn content of foraminifera might provide a valuable means to distinguish samples which may still contain the primary Cr signals recorded during shell formation. The overlap between some core-top and non-sedimentary specimens may provide a tool for assessing the impact of post-depositional incorporation of Cr into foraminiferal tests. Isotopic compositional changes related to size of the test may be caused by surface area/volume ratio effects on the exchange with Cr in pore and bottom waters.

Acknowledgements and author contributions

This work was supported by NERC GW4+ studentship 1509236 awarded to SR, by the Wolfson Research Merit Award from the Royal Society to DNS, by NWO large infrastructure subsidy 175.010.2009.011 awarded to JJM for the NanoSIMS facility, and by the Netherlands Earth System Science Center. The study was designed, and data were interpreted by SR, DNS, IJP and AYS. Laser ablation data were collected by AYS and SR. The work by AS was funded through ERC grant 2010-NEWLOG-ADG-267931 awarded to Professor Harry Elderfield. The culture studies were carried out by

SR and DT using facilities provided by SA. NanoSIMS analysis was carried out by AR, LP, MK and SR with the support of JJM. Plankton net and planktic foraminiferal culture samples were provided by KK, KAA and KH. Foraminiferal cleaning studies were conducted by SR, IJP and JS. SR, AYS, IJP, DNS, AR, LP and JJM wrote the manuscript. The authors would like to express their gratitude to Yiyi Jin, Mahzabeen Mahfuz, Florence Aves, and Sam Hammond for their invaluable assistance in the lab and would like to thank Gerald Ganssen and Barbara Donner for sharing samples. The authors also thank Wolfgang Kuhnt and Ann Holbourn for their assistance during the Sonne-185 cruise funded by the German Ministry of Education, Science and Technology (BMBF-grant 432 03G0185A, Sonne-185 cruise).

Appendix A. Supplementary material

Supplementary material related to this article can be found online at https://doi.org/10.1016/j.epsl.2019.03.001.

References

Allen, K.A., Hönisch, B., Eggins, S.M., Haynes, L.L., Rosenthal, Y., Yu, J., 2016. Trace element proxies for surface ocean conditions: a synthesis of culture calibrations with planktic foraminifera. Geochim. Cosmochim. Acta 193, 197–221. https://doi.org/10.1016/j.gca.2016.08.015.

Barker, S., Greaves, M., Elderfield, H., 2003. A study of cleaning procedures used for foraminiferal Mg/Ca paleothermometry. Geochem. Geophys. Geosyst. 4. https://doi.org/10.1029/2003GC000559.

Baturin, G.N., Dubinchuk, V.T., 2011. Mineralogy and chemistry of ferromanganese crusts. Geochem. Int. 49, 578–593. https://doi.org/10.1134/S0016702911060024.

Bonnand, P., Parkinson, I.J., James, R.H., Karjalainen, A.-M., Fehr, M.A., 2011. Accurate and precise determination of stable Cr isotope compositions in carbonates by double spike MC-ICP-MS. J. Anal. At. Spectrom. 26, 528. https://doi.org/10.1039/c0ja00167h.

Bonnand, P., James, R.H., Parkinson, I.J., Connelly, D.P., Fairchild, I.J., 2013. The chromium isotopic composition of seawater and marine carbonates. Earth Planet. Sci. Lett. 382, 10–20. https://doi.org/10.1016/j.epsl.2013.09.001.

Caromel, A.G.M., Schmidt, D.N., Phillips, J.C., Rayfield, E.J., 2014. Hydrodynamic constraints on the evolution and ecology of planktic foraminifera. Mar. Micropaleontol. 106, 69–78. https://doi.org/10.1016/j.marmicro.2014.01.002.

Cranston, R.E., Murray, J.W., 1978. The determination of chromium species in natural waters. Anal. Chim. Acta 99, 275–282. https://doi.org/10.1016/S0003-2670(01)83568-6.

Døssing, L.N., Dideriksen, K., Stipp, S.L.S., Frei, R., 2011. Reduction of hexavalent chromium by ferrous iron: a process of chromium isotope fractionation and its relevance to natural environments. Chem. Geol. 285, 157–166. https://doi.org/10.1016/j.chemgeo.2011.04.005.

Economou-Eliopoulos, M., Frei, R., Megremi, I., 2016. Potential leaching of Cr(VI) from laterite mines and residues of metallurgical products (red mud and slag): an integrated approach. J. Geochem. Explor. 162, 40–49. https://doi.org/10.1016/j.gexplo.2015.12.007.

Eggins, S.M., De Deckker, P., Marshall, J., 2003. Mg/Ca variation in planktonic foraminifera tests: implications for reconstructing palaeo-seawater temperature and habitat migration. Earth Planet. Sci. Lett. 212, 291–306. https://doi.org/10.1016/S0012-821X(03)00283-8.

Elderfield, H., 1970. Chromium speciation in seawater. Earth Planet. Sci. Lett. 9, 10–16. https://doi.org/10.1016/0012-821X(70)90017-8.

Ellis, A.S., Johnson, T.M., Bullen, T.D., 2002. Chromium isotopes and the fate of hexavalent chromium in the environment. Science 295 (5562), 2060–2062. https://doi.org/10.1126/science.1068368.

Erez, J., 2003. The source of ions for biomineralization in foraminifera and their implications for paleoceanographic proxies. Rev. Mineral. Geochem. 54, 115. https://doi.org/10.2113/0540115.

Farkaš, J., Frýda, J., Paulukat, C., Hathorne, E.C., Matoušková, Š., Rohovec, J., Frýdova, B., Francová, M., Frei, R., 2018. Chromium isotope fractionation between modern seawater and biogenic carbonates from the Great Barrier Reef, Australia: implications for the paleo-seawater δ^{53}Cr reconstruction. Earth Planet. Sci. Lett. 498, 140–151. https://doi.org/10.1016/j.epsl.2018.06.032.

Fehrenbacher, J.S., Russell, A.D., Davis, C.V., Gagnon, A.C., Spero, H.J., Cliff, J.B., Zhu, Z., Martin, P., 2017. Link between light-triggered Mg-banding and chamber formation in the planktic foraminifera *Neogloboquadrina dutertrei*. Nat. Commun. 8, 15441. https://doi.org/10.1038/ncomms15441.

Frei, R., Gaucher, C., Døssing, L.N., Sial, A.N., 2011. Chromium isotopes in carbonates — a tracer for climate change and for reconstructing the redox state of ancient seawater. Earth Planet. Sci. Lett. 312, 114–125. https://doi.org/10.1016/j.epsl.2011.10.009.

Frei, R., Paulukat, C., Bruggmann, S., Klaebe, R.M., 2018. A systematic look at chromium isotopes in modern shells – implications for paleo-environmental reconstructions. Biogeosciences 15, 4905–4922. https://doi.org/10.5194/bg-15-4905-2018.

Goring-Harford, H., Klar, J.K., Pearce, C.R., Connelly, D.P., Achterberg, E.P., James, R.H., 2018. Behaviour of chromium isotopes in the eastern sub-tropical Atlantic Oxygen Minimum Zone. Geochim. Cosmochim. Acta 236, 41–59. https://doi.org/10.1016/j.gca.2018.03.004.

Hatta, M., Measures, C.I., Wu, J., Roshan, S., Fitzsimmons, J.N., Sedwick, P., Morton, P., 2015. An overview of dissolved Fe and Mn distributions during the 2010–2011 U.S. GEOTRACES North Atlantic cruises: GEOTRACES GA03. Deep-Sea Res., Part 2, Top. Stud. Oceanogr. 116, 117–129. https://doi.org/10.1016/j.dsr2.2014.07.005.

Hemleben, C., Spindler, M., Anderson, O.R., 1989. Modern Planktonic Foraminifera. Springer-Verlag, New York.

Holland, K., Eggins, S.M., Hönisch, B., Haynes, L.L., Branson, O., 2017. Calcification rate and shell chemistry response of the planktic foraminifer *Orbulina universa* to changes in microenvironment seawater carbonate chemistry. Earth Planet. Sci. Lett. 464, 124–134. https://doi.org/10.1016/j.epsl.2017.02.018.

Holmden, C., Jacobson, A.D., Sageman, B.B., Hurtgen, M.T., 2016. Response of the Cr isotope proxy to Cretaceous Ocean Anoxic Event 2 in a pelagic carbonate succession from the Western Interior Seaway. Geochim. Cosmochim. Acta 186, 277–295. https://doi.org/10.1016/j.gca.2016.04.039.

Hönisch, B., Hemming, N. Gary, 2004. Ground-truthing the boron isotope paleo-pH proxy in planktonic foraminifera shells: partial dissolution and shell size effects. Paleoceanography 19, 1–13. https://doi.org/10.1029/2004PA001026.

Inoue, M., Nohara, M., Okai, T., Suzuki, A., Kawahata, H., 2004. Concentrations of trace elements in carbonate reference materials coral JCp-1 and giant clam JCt-1 by inductively coupled plasma-mass spectrometry. Geostand. Geoanal. Res. 28, 411–416. https://doi.org/10.1111/j.1751-908x.2004.tb00759.x.

Jacob, D.E., Wirth, R., Agbaje, O.B.A., Branson, O., Eggins, S.M., 2017. Planktic foraminifera form their shells via metastable carbonate phases. Nat. Commun. 8, 1265. https://doi.org/10.1038/s41467-017-00955-0.

Jochum, K.P., Weis, U., Stoll, B., Kuzmin, D., Yang, Q., Raczek, I., Jacob, D.E., Stracke, A., Birbaum, K., Frick, D.A., Günther, D., Enzweiler, J., 2011. Determination of reference values for NIST SRM 610–617 glasses following ISO guidelines. Geostand. Geoanal. Res. 35, 397–429. https://doi.org/10.1111/j.1751-908x.2011.00120.x.

Keeling, R.E., Körtzinger, A., Gruber, N., 2010. Ocean deoxygenation in a warming world. Annu. Rev. Mar. Sci., 199–229. https://doi.org/10.1146/annurev.marine.010908.163855.

Li, H., Xin, H.L., Kunitake, M.E., Keene, E.C., Muller, D.A., Estroff, L.A., 2011. Calcite prisms from mollusk shells (Atrina Rigida): Swiss-cheese-like organic-inorganic single-crystal composites. Adv. Funct. Mater. 21, 2028–2034. https://doi.org/10.1002/adfm.201002709.

Ni, Y., Foster, G.L., Bailey, T., Elliott, T., Schmidt, D.N., Pearson, P., Haley, B., Coath, C., 2007. A core top assessment of proxies for the ocean carbonate system in surface-dwelling foraminifers. Paleoceanography 22, PA3212. https://doi.org/10.1029/2006PA001337.

Palmer, M.R., 1985. Rare earth elements in foraminifera tests. Earth Planet. Sci. Lett. 73, 285–298. https://doi.org/10.1016/0012-821x(85)90077-9.

Paulukat, C., Døssing, L.N., Mondal, S.K., Voegelin, A.R., Frei, R., 2015. Oxidative release of chromium from Archean ultramafic rocks, its transport and environmental impact – a Cr isotope perspective on the Sukinda Valley Ore District (Orissa, India). Appl. Geochem. 59, 125–138. https://doi.org/10.1016/j.apgeochem.2015.04.016.

Paulukat, C., Gilleaudeau, G.J., Chernyavskiy, P., Frei, R., 2016. The Cr-isotope signature of surface seawater — a global perspective. Chem. Geol. 444, 101–109. https://doi.org/10.1016/j.chemgeo.2016.10.004.

Pereira, N.S., Voegelin, A.R., Paulukat, C., Sial, A.N., Ferreira, V.P., Frei, R., 2016. Chromium-isotope signatures in scleractinian corals from the Rocas Atoll, tropical South Atlantic. Geobiology 14, 54–67. https://doi.org/10.1111/gbi.12155.

Polerecky, L., Adam, B., Milucka, J., Musat, N., Vagner, T., Kuypers, M.M., 2012. Look@NanoSIMS – a tool for the analysis of nanoSIMS data in environmental microbiology. Environ. Microbiol. 14, 1009–1023. https://doi.org/10.1111/j.1462-2920.2011.02681.x.

Reinhard, C.T., Planavsky, N.J., Wang, X.L., Fischer, W.W., Johnson, T.M., Lyons, T.W., 2014. The isotopic composition of authigenic chromium in anoxic marine sediments: a case study from the Cariaco Basin. Earth Planet. Sci. Lett. 407, 9–18. https://doi.org/10.1016/j.epsl.2014.09.024.

Rodler, A., Sánchez-Pastor, N., Fernández-Díaz, L., Frei, R., 2015. Fractionation behavior of chromium isotopes during coprecipitation with calcium carbonate: implications for their use as paleoclimatic proxy. Geochim. Cosmochim. Acta 164, 221–235. https://doi.org/10.1016/j.gca.2015.05.021.

Saad, E.M., Sun, Y., Chen, S., Borkiewicz, O.J., Zhu, M., Duckworth, O.W., Tang, Y., 2017. Siderophore and organic acid promoted dissolution and transformation of Cr(III)–Fe(III)-(oxy)hydroxides. Environ. Sci. Technol. 51, 3223–3232. https://doi.org/10.1021/acs.est.6b05408.

Sadekov, A., Eggins, S.M., De Deckker, P., Kroon, D., 2008. Uncertainties in seawater thermometry deriving from intratest and intertest Mg/Ca variability in *Globigerinoides ruber*. Paleoceanography 23, PA1215. https://doi.org/10.1029/2007PA001452.

Scheiderich, K., Amini, M., Holmden, C., Francois, R., 2015. Global variability of chromium isotopes in seawater demonstrated by Pacific, Atlantic, and Arctic Ocean samples. Earth Planet. Sci. Lett. 423, 87–97. https://doi.org/10.1016/j.epsl.2015.04.030.

Schmidt, D.N., Elliott, T., Kasemann, S.A., 2008. The influences of growth rates on planktic foraminifers as proxies for palaeostudies – a review. In: Biogeochemical Controls on Palaeoceanographic Environmental Proxies. In: Geol. Soc. (Lond.) Spec. Publ., vol. 303, pp. 73–85.

Schmidtko, S., Stramma, L., Visbeck, M., 2017. Decline in global oceanic oxygen content during the past five decades. Nature 542 (7641), 335–339. https://doi.org/10.1038/nature21399.

Schoenberg, R., Zink, S., Staubwasser, M., Von Blanckenburg, F., 2008. The stable Cr isotope inventory of solid earth reservoirs determined by double spike MC-ICP-MS. Chem. Geol. 249, 294–306. https://doi.org/10.1016/j.chemgeo.2008.01.009.

Schroeder, D., Lee, G.F., 1975. Potential transformations of chromium in natural waters. Water Air Soil Pollut. 4, 355–365.

Semeniuk, D.M., Maldonado, M.T., Jaccard, S.L., 2016. Chromium uptake and adsorption in marine phytoplankton – implications for the marine chromium cycle. Geochim. Cosmochim. Acta 184, 41–54.

Soldati, A.L., Jacob, D.E., Glatzel, P., Swarbrick, J.C., Geck, J., 2016. Element substitution by living organisms: the case of manganese in mollusc shell aragonite. Sci. Rep. 6, 22514. https://doi.org/10.1038/srep22514.

Stramma, L., Oschlies, A., Schmidtko, S., 2012. Mismatch between observed and modeled trends in dissolved upper-Ocean oxygen over the last 50 years. Biogeosciences 9, 4045–4057. https://doi.org/10.5194/bg-9-4045-2012.

Tang, Y., Elzinga, E.J., Lee, Y.J., Reeder, R.J., 2007. Coprecipitation of chromate with calcite: batch experiments and x-ray absorption spectroscopy. Geochim. Cosmochim. Acta 71, 1480–1493. https://doi.org/10.1016/j.gca.2006.12.010.

Tang, Y., Marc Michel, F., Zhang, L., Harrington, R., Parise, J.B., Reeder, R.J., 2010. Structural properties of the Cr(III)–Fe(III) (oxy)hydroxide compositional series: insights for a nanomaterial 'solid solution'. Chem. Mater. 22, 3589–3598. https://doi.org/10.1021/cm1000472.

Titelboim, D., Sadekov, A., Almogi-Labin, A., Herut, B., Kucera, M., Schmidt, C., Hyams-Kaphzan, O., Abramovich, S., 2017. Geochemical signatures of benthic foraminiferal shells from a heat-polluted shallow marine environment provide field evidence for growth and calcification under extreme warmth. Glob. Change Biol. 23, 4346–4353. https://doi.org/10.1111/gcb.13729.

Troelstra, S.R., Ganssen, G.M., Sennema, E.J., Klaver, G.Th., Anderliesten, C., Van Den Borg, K., De Jong, A.M.F., 1987. Late Quaternary stratigraphy and sedimentology of the Central North Atlantic: a progress report. Nucl. Instrum. Methods Phys. Res., Sect. B, Beam Interact. Mater. Atoms 29, 317–321. https://doi.org/10.1016/0168-583X(87)90257-6.

Wang, X.L., Planavsky, N.J., Hull, P.M., Tripati, A.E., Zou, H.J., Elder, L., Henehan, M., 2017. Chromium isotopic composition of core-top planktonic foraminifera. Geobiology 15, 51–64. https://doi.org/10.1111/gbi.12198.

Wang, X.L., Reinhard, C.T., Planavsky, N.J., Owens, J.D., Lyons, T.W., Johnson, T.M., 2016. Sedimentary chromium isotopic compositions across the Cretaceous OAE2 at Demerara Rise Site 1258. Chem. Geol. 429, 85–92. https://doi.org/10.1016/j.chemgeo.2016.03.006.

Wei, W., Frei, R., Chen, T.-Y., Klaebe, R., Liu, H., Li, D., Wei, G.-Y., Ling, H.-F., 2018. Marine ferromanganese oxide: a potentially important sink of light chromium isotopes? Chem. Geol. 495, 90–103. https://doi.org/10.1016/j.chemgeo.2018.08.006.